Modeling of Subsonic Flow Through a Compact Offset Inlet Diffuser

Richard C. Jenkins* and Albert L. Loeffler Jr.†
Grumman Corporate Research Center, Bethpage, New York 11714

This paper presents a comparison of computational and experimental results that were obtained during an investigation of compressible flow through a compact, highly offset diffuser. Entrance values for the Mach number and the Reynolds number were 0.341 and $5.75(10)^5$, respectively. Strong curvature of the diffuser centerline produced extensive separation along one wall, which resulted in an exhaust flow with highly complex crossflow patterns and spatial nonuniformities. Our objective was to evaluate the use of an existing thin-layer Navier-Stokes code (ARC3D) to predict effects of diffuser shape and inlet flow properties on pressure recovery and exit flow quality. Comparisons are shown between computed and measured flow velocity components and wall pressure distributions. Agreement was satisfactory except in regions of separated flow. The Baldwin-Lomax algebraic turbulence model used in the code does not appear to represent adequately this complex separated region. We present preliminary results of computations made with a one-half-equation turbulence model, which accounts for some of the history effects in computing the turbulence length scale. The computed results show that the details of the axial velocity distribution in the separated flow region were quite different for the two turbulence models, but other features of the flow, such as the static pressure distributions, were only slightly affected.

Nomenclature

Cp = pressure coefficient, $= \left(\frac{P}{P_{si}} - 1\right) \Big/ \left(\frac{\gamma}{2} M_i^2\right)$
D = diffuser diameter
F_{Kleb} = Klebanoff intermittency correction, Eq. (4)
$F_{\max}$ = function defined by Eq. (3)
L = nonequilibrium turbulence length scale
M = local Mach number
P = static pressure
P_{si} = average value of inlet pressure
q = dynamic pressure
r = distance from wall
r^+ = $r\sqrt{\tau_w/\rho_w}/(\mu_w/\rho_w)$
Re = Reynolds number, based on diffuser inlet diameter
s = coordinate in direction of mean flow
U = mean velocity in x direction
u' = root-mean-square turbulence velocity in x direction
x = coordinate in direction of flow at diffuser entrance
x' = coordinate measured in x direction from start of curved portion of diffuser
y = coordinate measured horizontally from symmetry plane
y^+ = $y\sqrt{\tau_w/\rho_w}/(\mu_w/\rho_w)$
z = coordinate in vertical direction
γ = constant, 1.400
δ = boundary-layer thickness
μ = molecular viscosity
μ_t = turbulent viscosity
ρ = fluid density
τ_w = wall shear stress
ω = vorticity

Subscripts
e = exit plane
i = entrance plane
w = wall
x = in x direction
∞ = entrance, or edge of boundary layer

Presented as Paper 89-0639 at AIAA 27th Aerospace Sciences Meeting, Jan. 9-12, 1989, Reno, Nevada; received Jan. 30, 1989; revision received March 1, 1990.

*Senior Research Scientist. Member AIAA.
†Staff Scientist. Member AIAA.

Introduction

AIR induction systems for advanced aircraft include diffuser configurations that have a significant centerline curvature or offset. This diffuser shape produces complex crossflow patterns and nonuniform exit velocity profiles because of duct curvature. A conservative approach toward diffuser design employs analytical methods that deliberately restrict local wall curvature to a range that is separation-free.[1] Alternately, designers may proceed with a configuration that is known to develop some degree of flow separation and subsequently employ a corrective technique (e.g., suction, vanes, etc.) either to prevent separation or to suppress its effects.[2]

This paper presents a comparison of computational and experimental work that was undertaken to develop methods of modeling compact offset diffuser flows having extensive regions of internal flow separation. The total pressure recovery and the exit flow quality provided by an intake diffuser strongly influence engine thrust and compressor stall characteristics. Performance losses associated with highly offset diffusers depend on turbulent shear processes that occur in regions of separation and recirculation that are produced by the offset geometry. There is, at present, no adequate predictive method for this class of diffuser flows.

Our objective was to evaluate the capabilities of an existing thin-layer Navier-Stokes code for predicting the effects of diffuser shape and inlet flow properties on pressure recovery and exit flow quality. Flowfield computations were carried out with the ARC3D code (code obtained from NASA Ames Research Center). It is fully vectorized and for our application was solved on the CRAY XMP-14.

The diffuser geometry illustrated in Fig. 1 represents one of several diffuser models that were experimentally investigated for pressure recovery, flow quality, loss mechanisms, and performance improvement techniques for this general class of diffuser shape.[3] This diffuser model was chosen for an extensive series of experimental measurements to be compared with computed internal flowfield properties. Experimental mea-

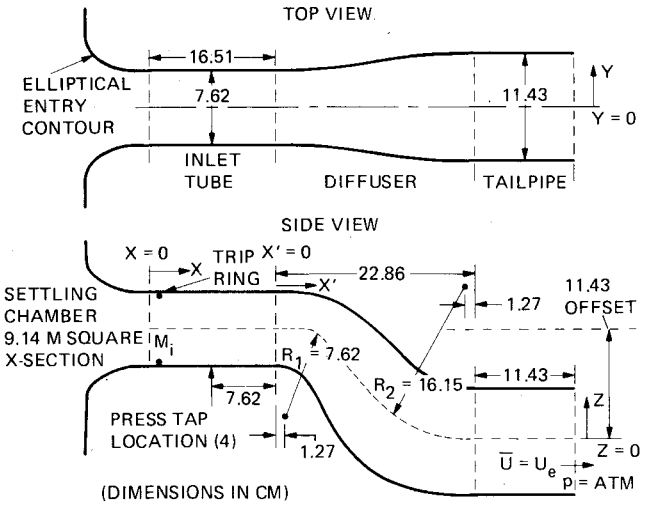

Fig. 1 Dimensions of offset diffuser model.

surements consisted of flowfield velocity with hot film X-probes and laser Doppler velocimetry (LDV), wall static pressure distributions, and wall streamline patterns using oil flow techniques.

Equations for Turbulence Models

The governing equations of mean motion are the same as given in Ref. 4, where the viscosity appearing in these equations has been replaced by the sum of the molecular and turbulent viscosities, namely $\mu + \mu_t$. The turbulence model used in the original ARC3D code is the Baldwin-Lomax[5] model. This model has been used extensively by earlier workers for attached or slightly separated flows and appears to be in good agreement with experiment. Near the wall, the model uses the well-known Prandtl-Van Driest formulation for the turbulent viscosity

$$(\mu_t)_{\text{inner}} = 0.16\rho r^2[1 - e^{(-r^+/26)}]^2|\omega| \tag{1}$$

In the region away from the wall

$$(\mu_t)_{\text{outer}} = 0.02688\ \rho F_{\text{Kleb}}(r) r_{\max} F_{\max} \tag{2}$$

where $r_{\max}$ and $F_{\max}$ are determined from the equation

$$F(r) = r|\omega|[1 - e^{(-r^+/26)}] \tag{3}$$

$F_{\max}$ is the maximum value of $F(r)$ that occurs in the profile, and $r_{\max}$ is the value of r at which it occurs. The r location where the inner and the outer regions meet is at the smallest value of r for which $(\mu_t)_{\text{inner}} = (\mu_t)_{\text{outer}}$. The value of F_{Kleb} is given by

$$F_{\text{Kleb}}(r) = \left[1 + 5.5\left(0.3\frac{r}{r_{\max}}\right)^6\right]^{-1} \tag{4}$$

For the massive flow separation occurring in our flow, it is not certain that a simple algebraic turbulence model such as the Baldwin-Lomax model is valid. A model accounting for upstream history effects on the turbulent viscosity would be more complete. The simplest model to do this is the one-half-equation model. Pletcher[6] used relaxation (or lag) arguments to arrive at the ordinary differential equation for the outer flow region

$$U_\infty \frac{dL}{dx} = 1.25\frac{\tau_w}{\rho_w}^{1/2}\frac{L}{\delta}\frac{\delta - L}{\delta} \tag{5}$$

The driving force in this equation is the difference between the nonequilibrium length L and the equilibrium length δ. Although Eq. (5) was derived for two-dimensional flow, we adapted the equation to our three-dimensional flow by substituting for δ the characteristic turbulence length predicted by the Baldwin-Lomax three-dimensional model and for dL/dx the derivative in the mean flow direction. The quantity L then becomes the nonequilibrium turbulence length scale that tends to approach the equilibrium Baldwin-Lomax value. In the inner region, Eq. (1) is again used.

Computer Code and Computer Facilities

The ARC3D computer code is based on the thin-layer Navier-Stokes equations and on the Beam-Warming implicit factorization algorithm.[7] The code takes compressibility fully into account, assuming the perfect gas law. The thin-layer form of the equations differs from the complete Navier-Stokes equations only by the neglect of the viscous derivatives parallel to the solid surface.[4] In many complex flow situations, such as the case we have treated, computer and cost limitations make it prohibitive to resolve these terms adequately if they are retained, due to the large number of grid points already used in the stretched grid perpendicular to the wall. Only recently has the ARC3D code been used to treat internal flows (e.g., Refs. 1 and 8). In our version of the ARC3D code, characteristic inflow boundary conditions have been applied[9] to minimize reflection of instability waves. The stagnation enthalpy, stagnation pressure, and direction cosines of the velocity vector are specified at the diffuser entrance; whereas, at the exit, atmospheric static pressure is specified.

In order to insure that our results were nearly grid-size-independent, we made several runs with a $40 \times 26 \times 24$ mesh; although most of our work was done using a mesh of $50 \times 32 \times 32$. Exponential stretching was used to obtain a fine mesh near the wall (mesh size adjacent to wall was about 0.0005 times the duct diameter). The two grid points nearest the wall were at values of y^+ of about 3.8 and 8.6 for our fine grid.

The front end of the CRAY XMP-14 system that we used was an IBM 3091. A typical completed computer run (with a grid of $50 \times 30 \times 30$) required 12,000 time increments that were equivalent to 5.51 CPU hr or 1.65 CPU s/time step. About 1.9 M central memory storage were needed for the grid. During the run, the averaged residuals were reduced by almost five orders of magnitude.

Experimental Equipment and Methods

A diffuser model with the same shape as that shown in Fig. 1 was investigated; it had a 7.62-cm-diam entrance and 11.43-cm-diam exit. The diffuser had parallel entrance and exit centerlines spaced (offset) 1 exit diam apart, a length of 2 exit diam, an area ratio of 2.25, and a circular cross-sectional shape normal to the curved centerline defined by two circular arcs that are mutually tangent near the diffuser midpoint. The diffuser cross-sectional area is essentially constant for 1 diam downstream of its entrance and then increases linearly to its exit. A constant area channel (designated the tailpipe) downstream of the diffuser exit served to straighten the exit flow.

The experiments were run as direct-connect tests with the diffuser entrance fed by a 7.62-cm-diam, 20.32-cm-long nozzle. The air supply was a 5.6-Kw motor and centrifugal fan used to pressurize a settling chamber designed for low turbulence level outflow. The turbulence intensity of the flow immediately upstream of the diffuser inlet was about 0.2%. An elliptical nozzle entry contour provided uniform velocity upstream of the diffuser entrance. A 0.0508-cm-thick trip ring, 0.508 cm long, was located just downstream of the nozzle entrance to assure turbulent boundary-layer conditions at the diffuser entrance. Four pressure taps were located around the periphery of the nozzle at a point 1 diam upstream of the diffuser entrance. The average value of these four measure-

ments (P_{si}) was taken as the diffuser entrance static pressure. The mean value of entrance dynamic pressure (q_i) was found from the settling chamber pressure and P_{si} using isentropic, compressible flow relations.

The experimental data were obtained with a diffuser entrance Mach number $M_i = 0.341$ and $Re = 5.75(10)^5$. A settling chamber pressure of 4.468 Kpa above atmospheric produced a $P_{si} = 3.723$ Kpa below atmospheric approaching the diffuser entrance, $q_i = 8.253$ Kpa, and a mean exit velocity $U_e = 49.68$ m/s. Wall surface pressure data are shown relative to the inlet static pressure and normalized by q_i in the form $(P - P_{si})/q_i$.

Surface pressure measurements were taken at 1.27-to-2.54-cm intervals along the upper, lower, and side walls of the diffuser, starting 1.27 cm downstream of the diffuser entrance. The transducers (Validyne Model CD15) were calibrated against a manometer. Data acquisition by an HP1000 computer included averaging of multiple values following analog to digital conversion. Comparison of different averaging techniques for data taken in the region of highest fluctuations (along the lower wall) suggests that the accuracy in mean value would be in the range of $C_p = \pm 0.02$ in this separated flow region. In regions where the flow is attached, the accuracy would be within $C_p = \pm 0.002$.

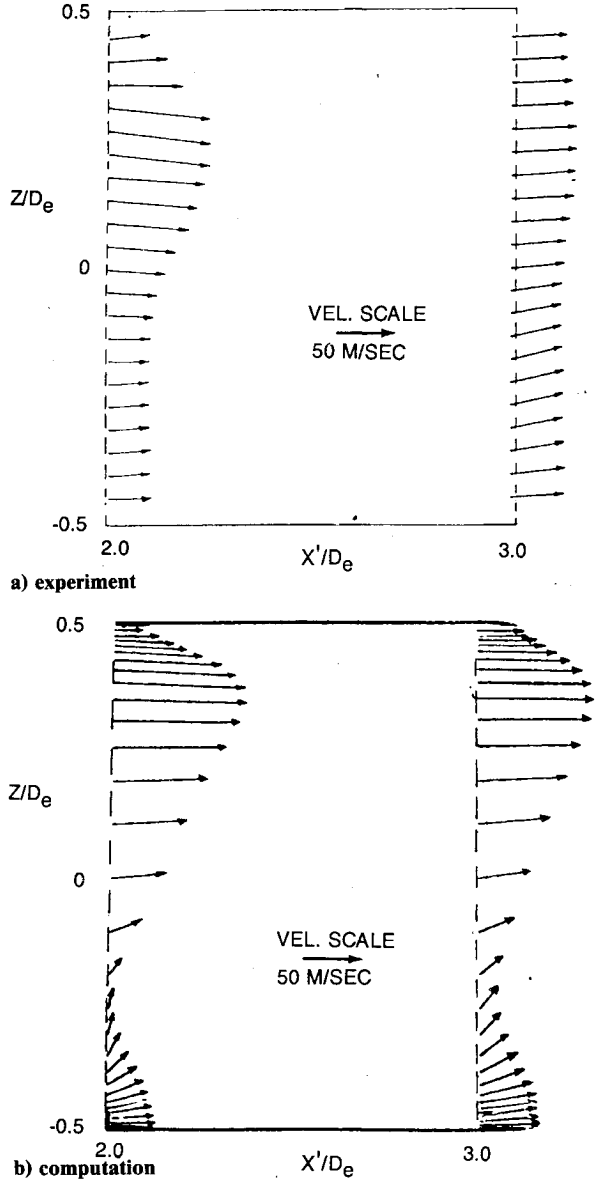

Fig. 2 Comparison of velocity profiles in symmetry plane at inlet and exit of tailpipe.

Velocities were measured with miniaturized hot film X-probes at the exit of the diffuser and within the tailpipe. TSI model 1050 constant temperature anemometers with linearized output were used to measure axial and transverse velocity components in two steps. A probe traverse across the flow measured one transverse component and the axial component at discrete points. A second traverse along the same path (with the probe measurement plane rotated 90 deg) obtained the orthogonal transverse component and a repeat of the axial component at the same points. Comparison of axial components taken in these two separate traverses generally showed agreement to within 1 percent difference.

An analysis of data accuracy suggests X-probe velocity data could be measured to within ± 2 m/s. Probe location could be measured by the traverse to within 0.1 mm. Combination of data from two traverses to develop secondary flow patterns would introduce a more significant error. Figures illustrating such patterns are intended only to compare the general nature of the crossflow behavior with predictions, so no length scale has been included on these figures.

A more dominant velocity error can exist at some points in the flow because of high turbulence levels. Although no upper limit on turbulence has been firmly established for X-probe measurements, it is generally accepted that data taken with u'/U greater than 0.4 will have a significant inaccuracy in mean value. Such conditions existed in the lower central region of the exhaust.

To address this source of error, we obtained measurements of axial velocity at the exit plane using a one-component LDV system operating in forward scatter. A Bragg cell was used so that data could be taken at high turbulence intensity. The seed material was propylene glycol. An atomizer produced nominally 2-μ diam droplets in the settling chamber about 0.6 m upstream of the diffuser entrance. At each measurement point, the data were obtained from 200 values taken at equal time intervals that were statistically analyzed to determine mean value and standard deviation. Accuracy of these data should be within 2 m/s.

Some general observations can be made concerning the flow pattern that develops in S-shaped channels and diffusers.[10,11] Centrifugal forces that develop in the initial bend produce crossflow velocity components directed toward the upper (compression) wall. Low-energy fluid moves outward along the upper wall and down the side walls, meeting downstream in the middle of the lower (expansion) wall; this, in turn, forms an upward crossflow component that promotes flow separation over an extensive region of the lower wall. Surface oil flow patterns[3] revealed that the downflow along the sides of the diffuser undergoes a reversal in direction, meeting from both sides on the lower line of symmetry to flow back upstream toward the point of initial separation. The separated

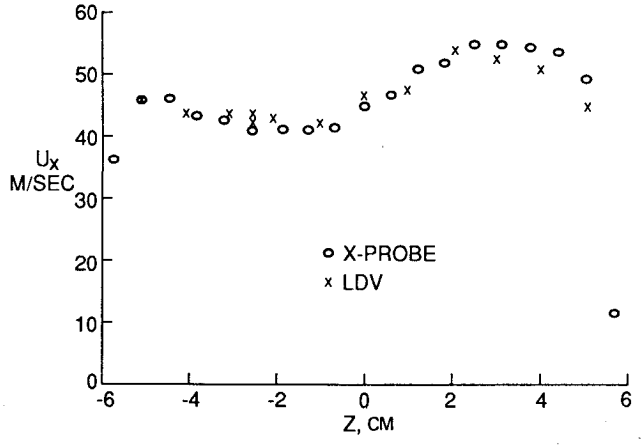

Fig. 3 Measured velocity component normal to exit in diffuser tailpipe symmetry plane.

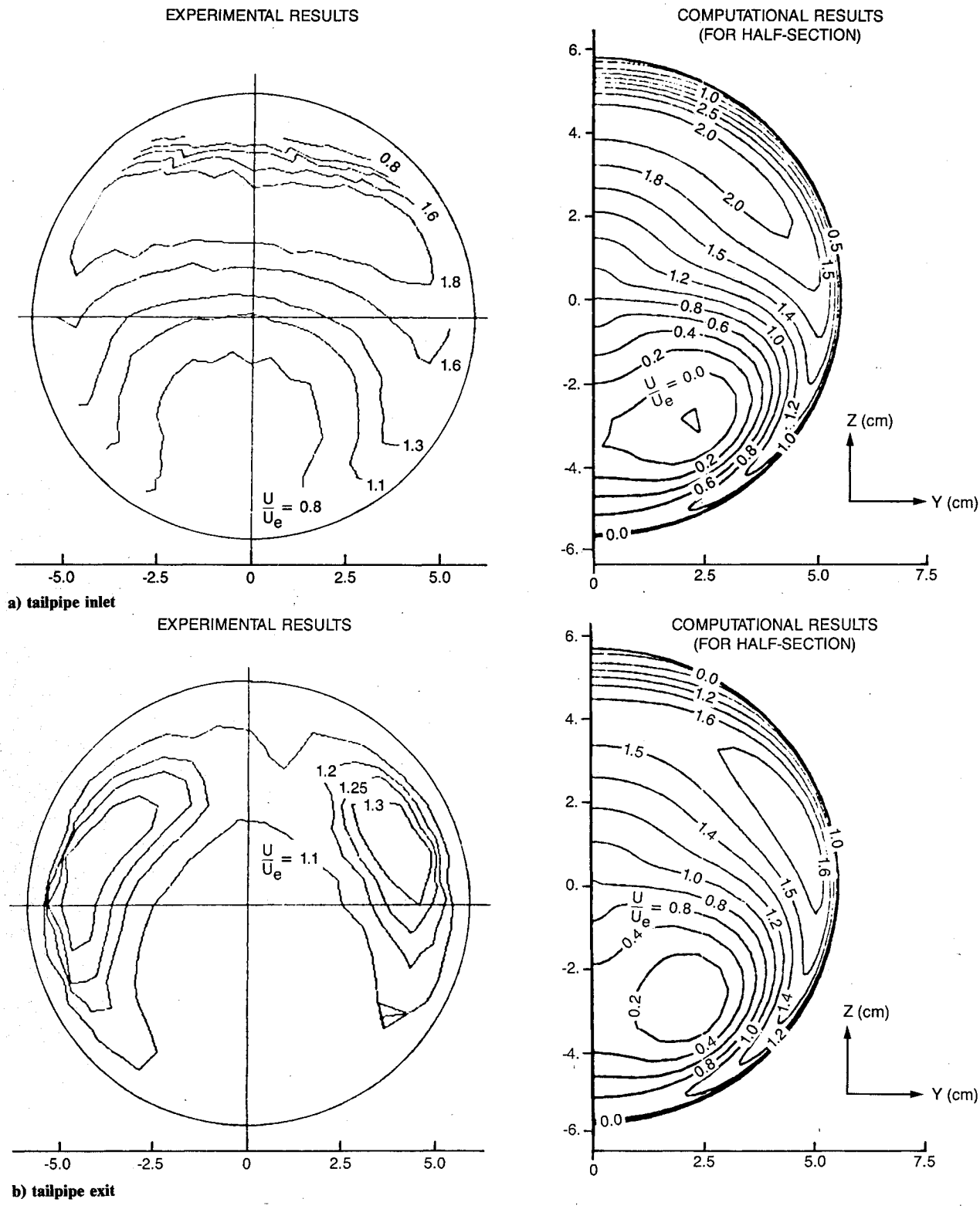

Fig. 4 Axial velocity contours in diffuser cross section.

flow was found to reattach to the lower wall shortly upstream of the tailpipe entrance.

Computational and Experimental Results

Using Baldwin-Lomax Turbulence Model

Velocity measurements taken in the plane of symmetry within the tailpipe are shown in Fig. 2a for comparison with computed profiles shown in Fig. 2b. Both the measured and the computed profiles show maximum velocities in the upper half and a minimum in the lower, but some differences are apparent. The computed profiles show velocities close to zero in the lower central region. A second difference is found by comparing changes that take place in the profiles at the tailpipe entrance and exit. Unlike the computed profiles, the experimental results show a smoothing of the profile as the flow passes through the tailpipe.

Figure 3 compares LDV and X-probe measurements of the velocity component normal to the exit plane of the diffuser tailpipe. LDV data taken at 12 points in the plane of symmetry at the exit showed close agreement with the X-probe measure-

ments. This experimental velocity check makes probe error an unlikely source of the disagreement between measured and predicted profiles in Fig. 2.

Figure 4a shows a comparison between experimental and computed values of the axial velocity components by means of contour plots in the plane of the tailpipe entrance. The velocities shown are normalized by the mean value of exit velocity. The upper part of the cross section shows good agreement, illustrating a curved layer of high-velocity flow above the centerline, which is consistent with the plane of symmetry profiles shown in Fig. 2. The lower central region of the cross section shows differences in the structure between the measured and the computed results. The computed flow shows a small region of flow reversal located off the plane of symmetry; while the X-probe measurements simply indicated a large region of low-energy flow in the lower central region.

Figure 4b shows a similar comparison in the plane of the tailpipe exit. The overall agreement between experiment and computation is closer here than at the tailpipe inlet. For example, the experimental isocontour line for $U/U_e = 1.1$ (the lowest experimental value) is very similar to an interpolated curve for $U/U_e = 1.1$ for the computed results. The only significant disagreement was found to be the prediction of off-center regions of almost zero velocity that were not found experimentally. LDV measurements taken throughout the lower region of the tailpipe verified the X-probe data.

The corresponding secondary flow patterns are compared at the tailpipe entrance and exit planes in Fig. 5. No velocity scale is shown here since the purpose of the figure is to indicate qualitatively the secondary flow patterns. Both experimental and computed plots at the entrance show a downflow pattern in the upper half and sides, forming an upflow from the lower central region and the beginning of a dual swirl pattern in the lower sides. Both also show that this swirl pattern intensifies as the flow passes through the tailpipe. One difference between experiment and computations consists of the experimentally observed progressive development of a strong upflow component in the lower central region, which is also evident in Fig. 2a. Another difference is seen in the exact location of the dual swirl pattern, which for the computed plot is slightly lower and at the same location as the minimum in the computed axial velocity contours in Fig. 4.

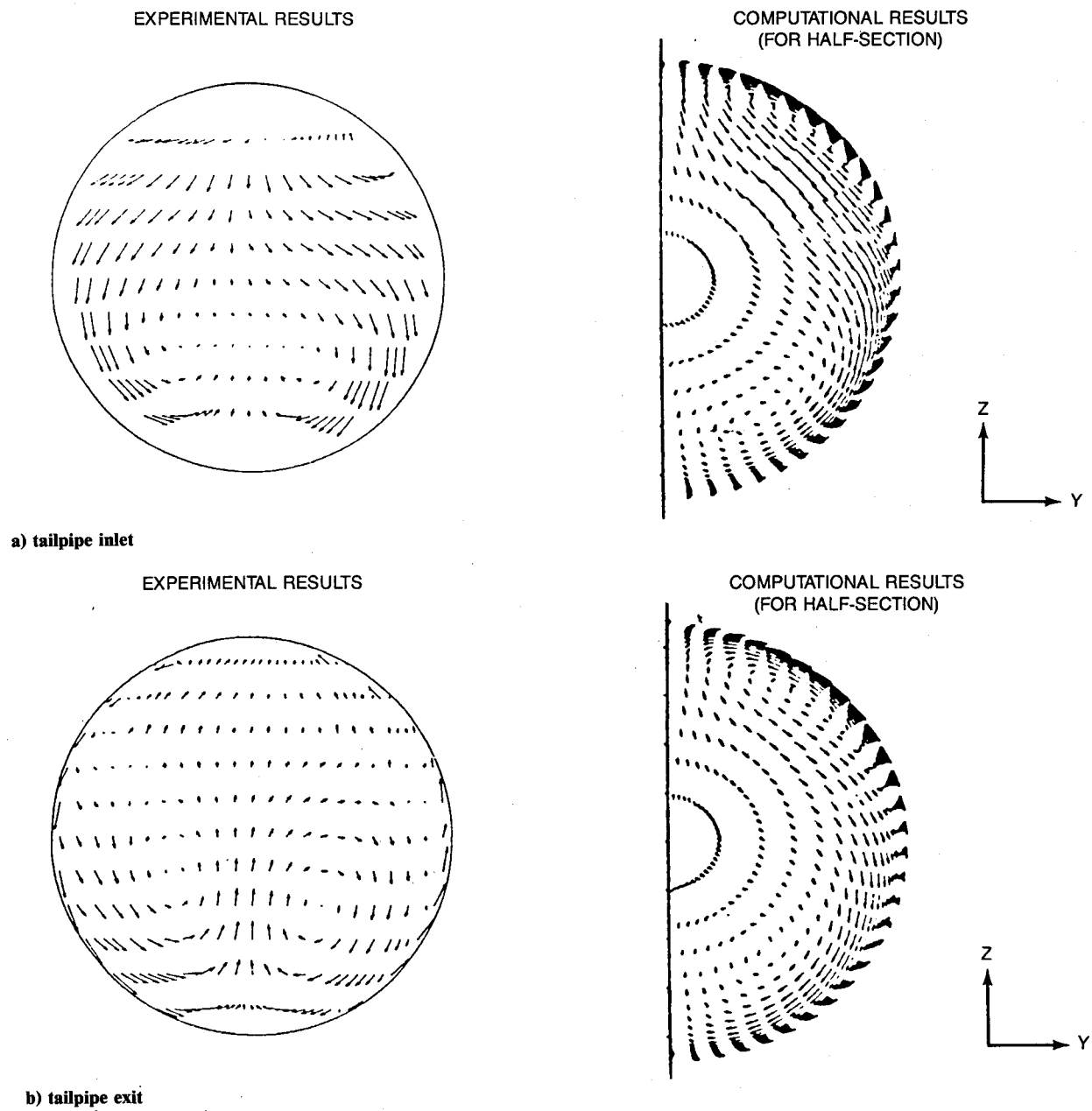

Fig. 5 Secondary flow pattern in diffuser cross section.

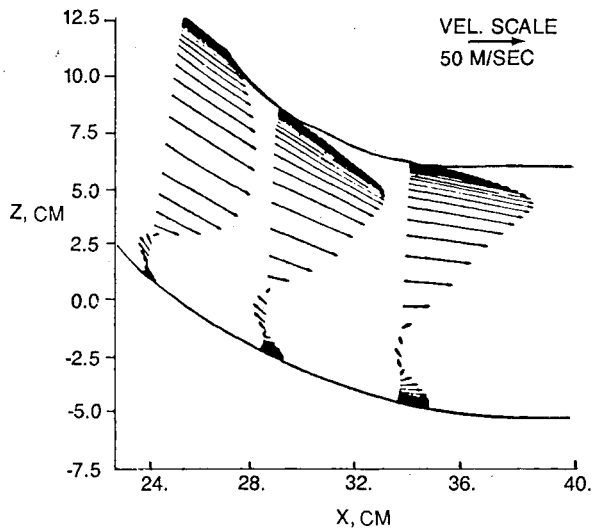

a) Baldwin-Lomax turbulence model

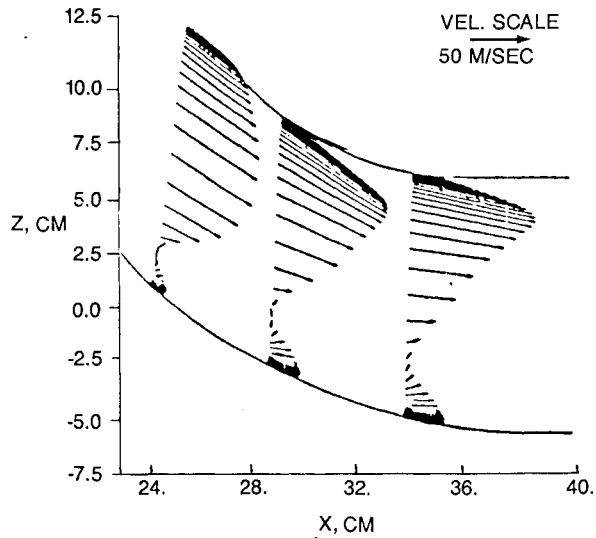

b) ½-equation turbulence model

Fig. 6 Velocity profiles at three axial stations in separated flow region.

Using a One-Half-Equation Turbulence Model

The velocity profiles shown in Fig. 6 in the vertical plane of symmetry illustrate one of the different characteristics computed for the separated flow region depending on the two turbulence models used. The Baldwin-Lomax model predicts a large region of flow reversal on the symmetry plane (Fig. 6a); while the one-half-equation model (Fig. 6b) predicts no significant flow reversal in this plane. It would appear, from consideration of the flow in the plane of symmetry, that the two turbulence models predict completely different behaviors for the region of separation.

A more balanced view of the effects of changing the turbulence model is obtained from contour plots of the computed axial velocity components given in Figs. 7a and 7b. These represent flow conditions at a cross-sectional location corresponding to the downstream profiles in Figs. 6a and 6b, respectively. The contour plots obtained using the two turbulence models are almost identical, showing reversed flow in symmetrically placed cells in the lower half of the cross section. However, the size of the separated region of this cell for the one-half-equation model is somewhat smaller, and, because of this, the region of reversed velocity does not extend to the plane of symmetry.

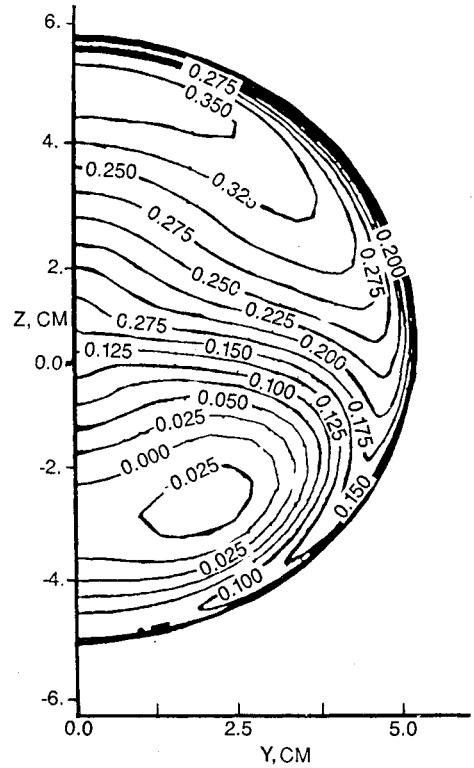

a) Baldwin-Lomax turbulence model

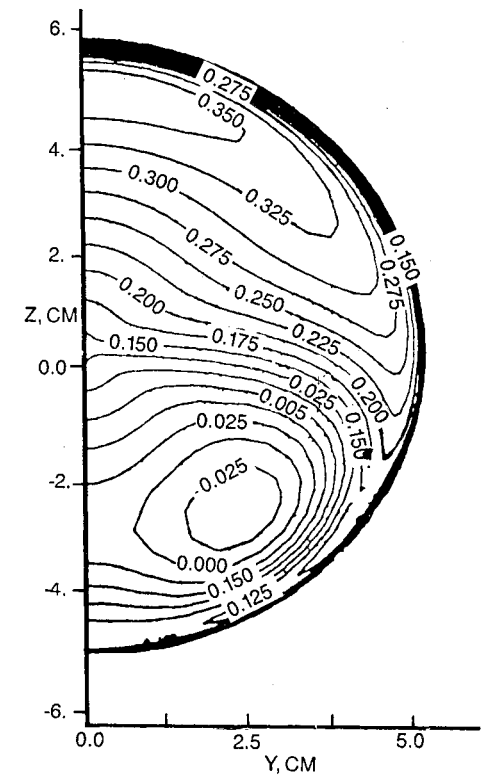

b) ½-equation turbulence model

Fig. 7 Computed axial velocity contours in half-sectional plane near downstream end of separated region.

Wall pressure data are shown in Fig. 8 in the nondimensional form C_p, plotted vs distance from the diffuser entrance. The dimension X' is measured parallel to X and has its origin at the onset of diffuser centerline curvature. The lower wall pressure distribution shows an initial rapid pressure rise when the flow separates from the wall between the first and the

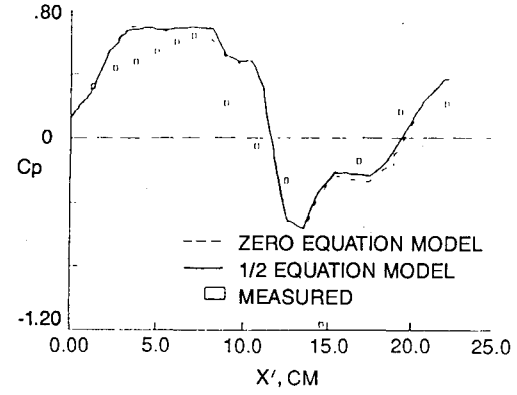

a) compression (upper) wall

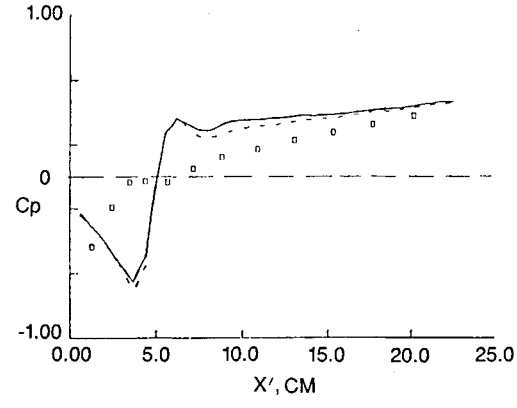

b) expansion (lower) wall

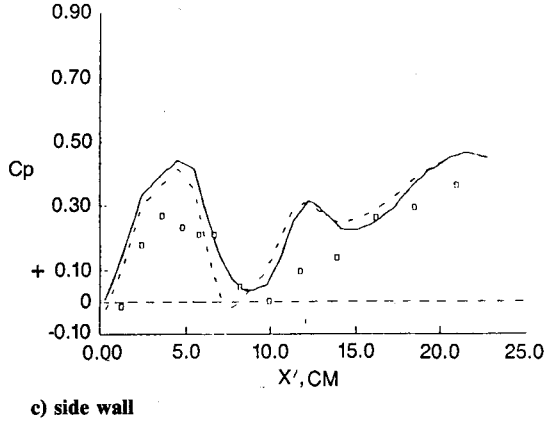

c) side wall

Fig. 8 Effect of turbulence model on variation of wall static pressure coefficient in flow direction.

second taps. The pressure plateau associated with separation ends with a compression caused by flow turning near the reflex in lower wall curvature. The side wall pressure distribution indicates separation at about the same axial location as the lower wall, but the downstream part of this plot resembles the upper wall pressure distribution. The rapid initial pressure rise on the upper wall appears to develop because of flow turning and ends when the upper wall reflex begins.

Shown for comparison are the wall pressure distributions predicted with the ARC3D code. There are essentially no differences between the wall pressure distributions predicted with the two turbulence models. The important trends of the experimental results are predicted only qualitatively. Agreement is somewhat closer along the compression wall where there is no flow separation. The computer code correctly predicts the existence of a nonuniform azimuthal pressure distribution at the onset of diffuser curvature.

In our opinion, the disagreement between experimental and computational results seen in the foregoing figures is caused by the inability of either turbulence model to describe adequately the massive separation and reattachment occurring in the experiment. For example, the actual flow separates much earlier (at $x' \cong 2$) than predicted by computation ($x' \cong 4$) as seen in Fig. 8b. The two turbulence models used are identical in the inner region (near the wall), and this region probably needs more accurate treatment.

Concluding Remarks

The flowfield found at the exit of a compact offset diffuser can be characterized by a noticeable drop in mean total pressure, by strong gradients in the axial velocity component and by a dual-swirl pattern in the crossflow velocity components. All of these characteristics are detrimental to the operation of a jet engine compressor, and all are traceable to the region of flow separation that develops in response to diffuser centerline curvature.

Using either turbulence model (Baldwin-Lomax or one-half-equation), the ARC3D computer program was found to be capable of predicting most of the major features that were measured in the diffuser flowfield. However, a noticeable difference was found between measured and predicted pressure distributions along the inner diffuser walls. These were the only measurements that were taken within the curved portion of the diffuser. This difference indicates a failure of the code to model adequately the flow close to the wall in the region of separation. It is interesting to note that a change to the more sophisticated one-half-equation turbulence model noticeably changed the computed flow pattern in the separation region, but had only a slight effect on the computed wall pressure distribution. As discussed earlier in relation to the results presented in Fig. 4, there also was considerable disagreement between experiment and computations (using the Baldwin-Lomax turbulence model) in the velocity details of the low-speed and reversed flow region at the tailpipe entrance.

We conclude that the ARC3D code provides a reasonably good representation of the flow at the exit of a compact, offset-axis diffuser and of the major flow features within the diffuser; however, the code does not accurately describe the separated flow region or the wall pressure detail within the diffuser.

In this paper, we have presented a limited number of computational results using the one-half-equation turbulence model. It will be necessary to use a more complex turbulence model, including a more realistic treatment of the region near the wall, to properly treat the extensive region of flow separation in compact, offset diffusers.

Acknowledgments

The authors appreciate the assistance provided by George Esposito in many phases of the computational work and that of George Homfeld in diffuser model construction and other phases of the experimental work. This work was performed under the Grumman Independent Research and Development program. The ARC3D code was obtained from the NASA Ames Research Center.

References

[1]Tindell, R. H., "Highly Compact Inlet Diffuser Technology," AIAA Paper 87-1747, June 1987.

[2]Maciulaitis, A., "Review and Critique of Papers on Diffuser and Engine Inlet Design," Grumman Corporate Research Center, Bethpage, NY, Memorandum RM-763, Jan. 1983.

[3]Jenkins, R., "Experimental Investigation of the Performance of Compact S-Shaped Diffusers," Grumman Corporate Research Center, Bethpage, NY, Rpt. RM-835, Nov. 1985.

[4]Anderson, D. A., Tannehill, J. C., and Pletcher, R. H., "Computational Fluid Mechanics and Heat Transfer," McGraw-Hill, New York, 1984, pp. 421-424.

[5]Baldwin, B. S., and Lomax, H., "Thin Layer Approximation and Algebraic Model for Separated Turbulent Flows," AIAA Paper 78-257, Jan. 1978.

[6]Pletcher, R. H., "Prediction of Incompressible Turbulent Separating Flow," *Journal of Fluids Engineering*, Vol. 100, Dec. 1978, pp. 427–433.

[7]Pulliam, T. H., "Euler and Thin Layer Navier-Stokes Codes: ARC2D, ARC3D," *Notes for Computational Fluid Dynamics Users' Workshop*, Univ. of Tennessee Space Institute, Tullahoma, TN, March 1984.

[8]Davis, W. H., "Applied Transonics at Grumman," Transonics Symposium, NASA Langley Research Center, April 1988.

[9]Davis, W. H., Aircraft Systems Div., Grumman Corp., private communication, Oct. 1987.

[10]Bansod, P., and Bradshaw, P., "The Flow in S-Shaped Ducts," *Aeronautical Quarterly*, Vol. 23, May 1972, pp. 131–140.

[11]Aulehla, F., "Intake Swirl—A Major Disturbance Parameter in Engine/Intake Compatibility," *Proceedings of 13th Congress of ICAS and AIAA Aircraft Systems and Technology Conference*, AIAA, New York, Aug. 1982.